

Quantitative local current-voltage analysis and calculation of performance parameters of single solar cells in modules

J. Bauer*, F. Fröhlauf, O. Breitenstein

Max Planck Institute of Microstructure Physics, Weinberg 2, 06120 Halle, Germany



ARTICLE INFO

Article history:

Received 6 July 2016

Received in revised form

24 August 2016

Accepted 27 August 2016

Available online 8 September 2016

Keywords:

Current-voltage analysis

Modules

Si solar cells

Electroluminescence

Lock-in thermography

Single cell analysis

ABSTRACT

Quantitative characterization of single cells already embedded in modules is performed by a combination of electroluminescence imaging and dark lock-in thermography. Electroluminescence imaging is used to determine the terminal voltages of single cells in modules, and dark lock-in thermography imaging enables the use of quantitative analyses of single solar cells with the software Local I-V 2. This combination yields spatially resolved images of the performance parameters of single cells. To check the reliability of the method also the directly measured voltages of the single cells in a module have been used for Local I-V evaluation and are compared to the results of Local I-V evaluation from voltages determined by EL. The accuracy of the voltage determination in our experiments is about $\pm 1\%$ compared to directly measured voltages, leading to an accuracy of the cell parameters such as J_{01} , U_{oc} , efficiency, power, FF, and so on of about $\pm 2\%$ using the voltages determined by EL for the Local I-V analysis. With the method introduced it is possible to quantitatively identify the performance of single solar cells in modules reliably and non-destructively, thereby tracking quantitative changes of the cell performance due to degradation processes with high sensitivity and spatial resolution becomes possible.

© 2016 Elsevier B.V. All rights reserved.

1. Introduction

Solar cells can be investigated and characterized with a lot of standard methods, for example electro- and photoluminescence (EL/PL), lock-in thermography (LIT), light beam induced current (LBIC), and so on, all giving a map of a method-dependent parameter of the whole solar cell, see e.g. [1–6]. These images can be used for qualitative and in many cases even for quantitative analyses of solar cells. For the characterization of solar cells embedded in modules in principle the same methods can be used. Imaging methods for modules become more and more important for quality and reliability control of photovoltaic modules in terms of degradation, power yield, and hot spots. Different approaches to image loss mechanisms in solar modules have been published recently. Especially EL has been used due to its simplicity for imaging the degradation of cells in modules e.g. due to cracks and broken grid fingers [7–9], potential induced degradation (PID) [10–12], so called “LeTID” (light and elevated temperature induced degradation) [13], so called “snail trails/tracks” [14], and long term stability of modules [15]. Thermography (in steady-state and lock-in modus) imaging is used mainly to detect hot spots due to their nature of increased temperatures [16,17]. Also the analyses of

power losses due to PID using thermography images was shown recently [18]. To detect cracks, shunts and other defects in modules often a combination of EL imaging and infrared (IR) thermography is used, since EL has a much better spatial resolution compared to steady-state thermography and even to LIT [19–21]. Note that luminescence imaging and LIT perfectly supplement each other, since luminescence images the local diode voltages quantitatively and LIT images the local diode currents. Most of the above mentioned methods for modules are only qualitative investigations, even if they give spatially resolved images of the modules. Another attempt for non-destructive quantitative analysis of cells in modules was done by evaluating EL images [22]. Here the individual cell parameters such as the ideality factors $n_{1,2}$, and the dark saturation current densities $J_{01,02}$ of single cells in a module have been estimated by investigating the relationship between individual cell parameters of solar cells connected in series, the voltage dependent EL intensity, and the current-voltage (I - V) curve of the complete module [22]. However, this approach does only lead to global cell parameters and not to spatially resolved parameters of each single cell. For quantitative spatially resolved analyses of solar cells in modules the individual cell voltage, i.e. the terminal voltage, is necessary to know.

If it is required to apply a voltage to a cell in a module, for instance for EL and LIT measurements, the voltage can only be applied indirectly via all the other cells to the cell under test. In today's standard photovoltaic modules (60 or 72 cells per module)

* Corresponding author.

E-mail address: jbauer@mpi-halle.mpg.de (J. Bauer).

all cells are connected in series. Hence, the current through all the cells is the same and equals the module current I_{mod} . Unfortunately, the often made simplification that the individual cell voltages U_i (i =number of cells in the module) results from the module voltage U_{mod} divided by the number of cells N in the module does only hold if all cells would have exactly the same current-voltage characteristic, which is not the case in reality. Instead, U_i of each cell is adjusted individually (so-called floating voltages) and is determined by the I - V characteristic of the cell, because each cell shows a different voltage at I_{mod} . Hence, for characterizing a single cell in a module, the individual cell voltage at different working points, i.e. different I_{mod} has to be determined. This can be done by the approach reported by Köntges et al. [23] and Potthoff et al. [24] using the maximum EL signal of each cell in the module for determining the individual cell voltages.

The aim of our work is to get quantitative, spatially resolved data of the performance parameters of single solar cells in standard 60-cell modules using EL and dark lock-in thermography (DLIT) imaging. For this purpose we use the approach by Köntges and Potthoff, see [23,24], to get the single cell voltages at different working points and measure DLIT images at the same working points to apply the quantitative Local I-V evaluation of DLIT images [25–27] to single cells in a module, which is described in Sections 2.2 and 3.2.

2. Experimental and methods

For our investigations we use a standard 60-cell module made of PERC (passivated emitter and rear cell [28]) solar cells, which are specially treated to show a light- and elevated temperature-induced degradation effect. The module was degraded according to [13]. For our purposes we benefit from the fact that some cells show a strong degradation and other cells show no measurable degradation, hence a large variation in cell performance can be expected, and a large variation in cell voltages, which in turn is a good test for our investigation method. For testing our method we measure the cell voltages directly at the module as well. To be able to do so, the module was locally opened carefully on the rear side at the middle busbars between two cells, respectively, and contact wires have been soldered at these positions onto the middle busbars. The single cell voltages $U_{i,\text{meas}}$ have been measured with a multimeter with an error of about ± 0.2 mV. A similar approach was used by Köntges and Potthoff et al. in [23,24]. For applying voltage and current to the module the junction box was opened and four wires, two for the plus and minus contact, respectively, have been soldered onto the module contacts in the junction box. This allows four-point probing of the module preventing errors due to voltage drops caused by the external wiring, which might cause failures of the module voltage measurement.

Following the method published in [23,24] one needs the maximum EL signal of each cell to determine its terminal voltage, i.e. the voltage which can be measured at the metal contacts of the cell. For the quantitative DLIT analysis of the solar cells [25,26] DLIT images at three different voltages are needed. Here we restrict on forward bias investigations, since the Köntges/Potthoff method [23,24] works only under forward bias. Hence, if there should be ohmic shunts in the cells, they will be identified as J_{02} -type shunts with a large ideality factor. We performed EL imaging, DLIT imaging, and steady-state thermography imaging of the module, using a Si-CCD Sensovation CoolSamba HR-400 camera with a pixel resolution of 2048×2048 for EL imaging, and the Lock-in Thermography system PV-LIT by InfraTec equipped with an InSb detector camera (Image IR 8300) with a resolution of 640×512 pixels for the thermography measurements. For the voltage determination using the EL images, steady-state

Table 1
Global module parameters for cell voltage determination from EL images.

U_{mod} [V]	I_{mod} [A]	T_{mod} [K]	n_i [cm^{-3}] from [32]	C eq. (9)	R_{mod} eq. (4) [Ω]
33.85	0.627	297.2	7.76×10^9	3.46×10^{-7}	0 (per def.)
35.55	1.606	298.5	8.66×10^9	4.31×10^{-7}	0.242
37.27	3.800	302.0	1.16×10^{10}	7.70×10^{-7}	0.226
38.47	6.705	306.7	1.69×10^{10}	1.65×10^{-6}	0.224

Table 2
Global module parameters for DLIT measurements.

U_{mod} [V]	I_{mod} [A]	T_{mod} [K]	ΔT_{mod} EL–DLIT [K]
33.84	0.627	296.5	0.7
35.80	1.606	297.2	1.3
37.44	3.804	298.7	3.3
39.05	6.705	301.7	5

thermography images were needed to determine the temperatures of all cells as exact as possible, since during the high voltage (high current) measurements the cells get significantly warmer than the surrounding. As a consequence the current is rising until the thermal equilibrium to the surrounding is reached. To limit this effect, we operated the power supply in constant current mode to get approximately the desired U_{mod} , see details below in Tables 1,2. The accuracy of the current limit was better than ± 10 mA. The integration time for each EL image was 180 s.

DLIT was performed by imaging the back sheet of the rear side of the module at 1 Hz lock-in frequency for 1 h for each image. Therefore the LIT images contain the shadow of the junction box at the top. In the efficiency analysis only the non-shadowed part of the corresponding cells could be analyzed. All LIT based images are shown mirrored for a better comparison to the front side EL images. It is important to note that EL is done by applying a constant current to the module and DLIT is done by applying a pulsed current to the module. Hence, different power is consumed by the module at the same current limit and different temperatures are reached in thermal equilibrium to the environment, regarding a fixed current limit. Therefore it was important to measure the temperature as exactly as possible to be able to correct the cell voltages for the temperature differences between the EL and the DLIT measurements (see details in Section 3.2). We managed to measure the temperatures of each cell with an error of about ± 0.2 °C by IR imaging. We measure the module voltage with an error of about ± 0.01 V. Please note that the temperature change of the module depends strongly on the lab conditions such as air temperature, air flow (maybe due to an active air conditioning) and the lab size. We performed our measurement in an air conditioned lab with a nominal fixed temperature of about 20 °C, this gave us the opportunity to repeat measurement under nearly the same conditions.

Overall we took EL images, the corresponding thermography images for EL, and DLIT images at four different module voltages U_{mod} , please see Tables 1,2 for details. For EL a background image was taken at zero bias with the same integration time and subtracted from each EL image to get rid of bad pixels and background illumination. All measurements have been performed in a dark lab to minimize effects of the surrounding. The cells are named from 1 to 60 according to the scheme in Fig. 1(a).

2.1. Cell voltage determination by EL

The local EL signal $\Phi(x,y)$ of a solar cell depends on the local voltage $U(x,y)$ and the local calibration factor $C(x,y)$:

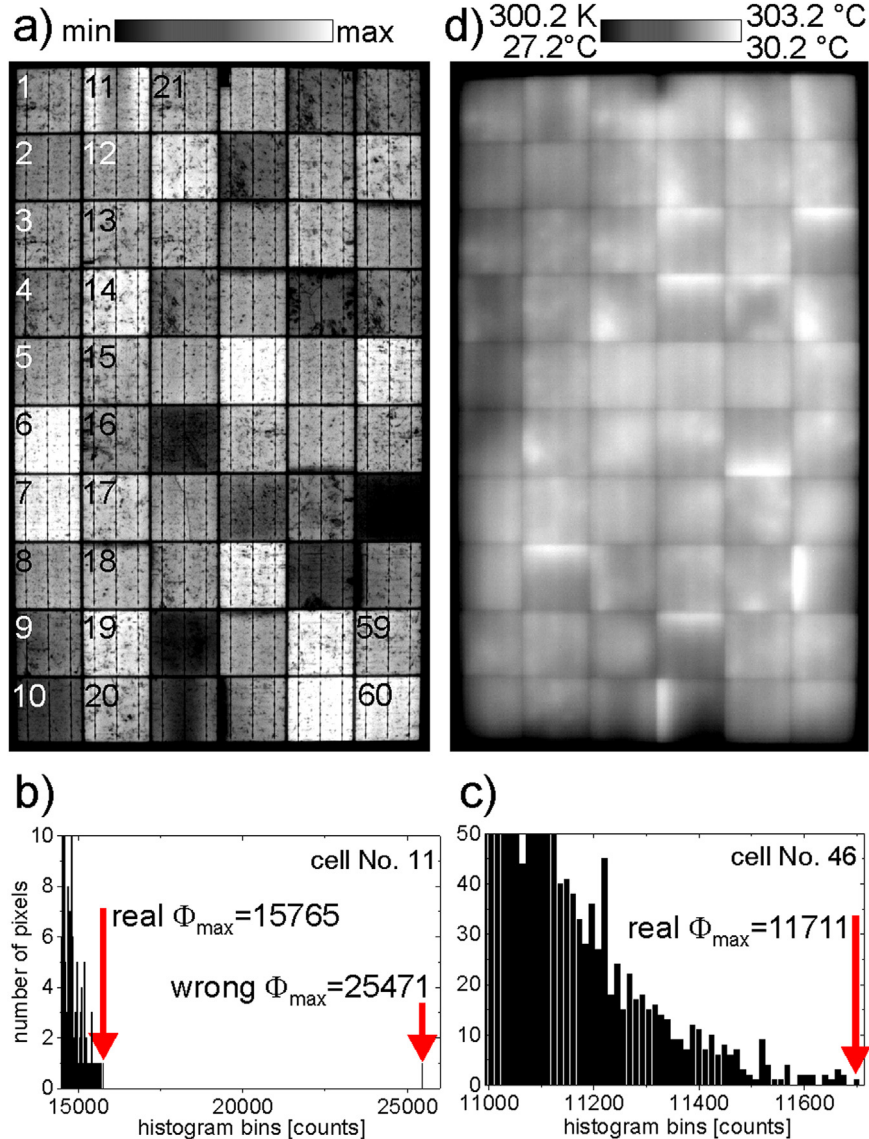


Fig. 1. a) EL image of the module taken at 37.27 V (3.8 A), b) and c) parts of the histograms of the EL images of cells No. 11 and 46. d) Thermography image of the module for determining the cell temperatures and the average module temperature. In a) the numbering scheme of the cells in the module is given (index i in the equations).

$$\phi(x, y) = C(x, y) \exp\left(\frac{U(x, y)}{kT/e}\right), \quad (1)$$

with kT/e being the thermal voltage, k the Boltzmann factor, T the temperature in Kelvin and e the electronic charge. Following the approach in [23,24] that at the brightest pixel $\Phi(x,y)_{\max}$ in a solar cell $U(x,y)$ represents the terminal voltage U (i.e. the voltage measured between the front and rear contact), Eq. (1) can be converted to

$$U = U(\phi(x, y)_{\max}) = \frac{kT}{e} \ln\left(\frac{\phi(x, y)_{\max}}{C(x, y)_{\max}}\right), \quad (2)$$

from which one can determine the terminal voltages of cells in modules from EL images. It is well-known that, with increasing bulk lifetime, the calibration factor reaches a limiting value [29,30]. It is assumed in [23,24] that each cell contains at least one region with such a sufficiently high lifetime and low series resistance. Therefore it can be assumed that $C(x,y)_{\max}$ is the same for all pixels showing maximal EL signal, hence $C(x,y)_{\max}=C$ holds. This assumption is well justified since the optical and material

properties at the brightest pixels in each cell can be estimated to be nearly equal. Following [23,24] C can be calculated out of a measurement at a low voltage where $I_{\text{mod}} < 0.1I_{\text{sc}}$ (I_{sc} =short circuit current), because the module series resistance R_{mod} can be neglected due to the low current and C can be calculated as follows (for such low U_{mod} where $I_{\text{mod}} < 0.1I_{\text{sc}}$):

$$C = \sqrt{\frac{\prod_{i=1}^N \phi_i(x, y)_{\max}}{\exp\left(\frac{U_{\text{mod}}}{kT/e}\right)}}. \quad (3)$$

To determine the cell voltages at higher voltages (currents) series resistance effects have to be taken into account. Normally the brightest pixels in a cell are found in high lifetime areas close to the busbars where the local internal series resistance $R(x,y)_{\text{int}}$ in a cell is small and can be neglected [23]. However, for calculating the terminal voltage U of the cell one has to consider the resistance of the cell interconnectors and the resistance of the solar cell material itself (called external resistance R_{ext} in [23,24]). By subtracting the sum of all terminal voltages of the cells U_i ($i=1-N$, $i=\text{cell number}$) in a module from the measured module voltage

U_{mod} divided by the module current I_{mod} and using Eq. (2) for each cell voltage U_i one gets the module resistance R_{mod} :

$$R_{\text{mod}} = \frac{1}{I_{\text{mod}}} \left(U_{\text{mod}} - \sum_{i=1}^N \frac{kT_i}{e} \ln \left(\frac{\phi_i(x, y)_{\text{max}}}{C} \right) \right). \quad (4)$$

with T_i being the individual cell temperature taken from the thermography image for each module voltage (see e.g. Fig. 1(d) for $U_{\text{mod}}=37.27$ V). T_i is the average temperature of the area of each cell. This is a small difference to [23,24] where the module temperature was measured at one point in the middle of the module. The external resistance of one cell is then

$$R_{\text{ext}} = \frac{R_{\text{mod}}}{N}. \quad (5)$$

Eq. (5) is only valid if the assumption is made that all interconnectors have the same series resistance and that the contact resistances between cell interconnectors and cells are equal as well [23,24]. Regarding the external resistance and the assumption $C(x,y)_{\text{max}}=C U_i$ calculates finally to [23,24]:

$$U_i = \frac{kT_i}{e} \ln \left(\frac{\phi_i(x, y)_{\text{max}}}{C} \right) + R_{\text{ext}} I_{\text{mod}}. \quad (6)$$

Note that C is strongly temperature-dependent. In [23] C was determined using the EL maxima values of the measurement with the lowest U_{mod} after (3) at approximately room temperature. The radiative emission of solar cells (i.e. the luminescence signal) depends on the square of the intrinsic carrier density n_i [1], which is strongly temperature dependent [31,32]. Measurements at higher module voltages lead to temperature increase of the module and thereby to increased intrinsic carrier density. Therefore, in [23] it was proposed to correct C for the temperature effect by

$$C = n_i^2 B, \quad (7)$$

with n_i being the intrinsic carrier density and B the temperature independent radiative recombination coefficient. With known C and n_i from the low voltage measurement from (3), B can be calculated and then used for the C correction at higher temperatures using the corresponding n_i values [23]. While in [23,24] the temperatures were measured by a thermocouple, we are measuring them by IR thermography. Please note that for the calculation of C in Eq. (3) and of n_i^2 in Eq. (7) the average module temperature for each module voltage is used, respectively. Hence, C is constant for all cells for each module voltage.

2.2. Lock-in measurements and local I-V principle on module level

In this section we want to describe briefly how we perform the Local I-V analysis on single cells on module level in principle. The results will be found in the next section. For the local analysis of single solar cells after Breitenstein at least three DLIT images at different forward biases are necessary [25,26]. For this purpose we use the DLIT -90° images taken of the module at the three higher module voltages given in Table 2 and selected the image of each single cell for each voltage image. We use the three higher voltages since the DLIT image of the lowest voltage contained still too much noise, hence the results would be error-prone due to the DLIT measurement. By using the cell voltages U_i for each cell determined by the approach described in Section 2.1 for each module voltage, we can perform a Local I-V analysis of a single cell. The DLIT -90° images of each cell, $T^{-90^\circ}(x,y)$, are converted into power density P_i images by applying [25,26]

$$P_i(x, y) = \frac{T^{-90^\circ}(x, y)(U_i - R_s I(x, y)) I_{\text{mod}}}{\langle T^{-90^\circ}(x, y) \rangle A}, \quad (8)$$

with $\langle T^{-90^\circ}(x, y) \rangle$ being the average temperature modulation of the whole cell area, R_s is the series resistance of the cell, $I(x,y)$ is the current at each pixel which is known from the DLIT images, and A is the cell area. From (8) current density maps $J(x,y)$ are derived since voltage and current of the cell are known from the EL analysis and the module currents. Each pixel (i.e. the same pixel for the three different voltages) of the current density maps of the solar cell is fitted to a two-diode model assuming $n_1=1$ and n_2 variable with a homogeneous series resistance of $0.7 \Omega \text{ cm}^2$ (which turned out to be a good approximation), giving the dark I-V curve of each pixel with the parameters J_{01} , J_{02} , $n_1=1$ and n_2 . Summing up all pixels gives the global I-V curve of each single solar cell. From these dark I-V curves the illuminated I-V curves of the cells are calculated to determine maps of the solar cell parameters such as efficiency, FF, U_{oc} and so on. For this calculation we use a constant short circuit current of $J_{\text{sc}}=38.5 \text{ mA/cm}^2$, which was taken from the flasher measurement of the module. For the Local I-V procedure in detail please see [25,26].

Please note: since not all cells in the module show the same series resistance, and of course not the same short circuit current, the above mentioned fitting parameters are approximations, hence our results show a certain error due to the choice of these parameters. However, at least J_{sc} is a good guess because we know the module's J_{sc} . Note further: since it is not possible to take reliable DLIT images of photovoltaic (PV) modules under reverse voltage, no ohmic shunts are considered in the Local I-V evaluation. Due to the resolution of 640×512 pixels of our LIT camera each cell is mapped with a pixel resolution of about 60×60 pixels if we image the whole module, which is still enough to see some details as will be shown in the next section. By combining the maps of the efficiency or U_{oc} (or others) of all cells, we obtain maps of the whole module but showing the individual map of each cell (and each cell with a resolution of 60×60 pixel in our case).

3. Results

3.1. Cell voltages from EL and direct measurements

In Fig. 1(a) an EL image of the module is shown as an example. This image was taken at $U_{\text{mod}}=37.27$ V with $I_{\text{mod}}=3.8 \text{ A}$ at nominal mean module temperature of 302.0 K (29.0° C). From each cell of the module the maximum EL signal Φ_{max} was taken. To avoid using outliers, despite subtracting background images, the histogram of each cell area has been checked. To illustrate the problem by an example, parts of the histograms of the EL images of cells No. 11 and 46 taken from image a) are shown in Fig. 1(b) and (c), respectively. In cell 11 an outlier of approx. 25,500 counts is found, which must be ignored, the real Φ_{max} of this cell was found to be 15,765. The histogram of cell 46 does not show any outliers, hence the maximum value was directly used for the voltage determination. Please note that in [23,24] 0.1% of all camera pixels showing the highest standard deviation have been excluded to regards outliers. In Fig. 1(d) the thermogram corresponding to the EL image is shown. It is obvious that the temperature even within one cell's area is not homogeneous, hence for the voltage calculation the average temperature is determined for each cell and used for kT/e . Using the average cell temperature is justified by the fact that the dark areas in the EL image in Fig. 1(a) are the areas showing the highest temperatures in Fig. 1(d) and it is very unlikely that Φ_{max} is taken from such a high temperature position in the cell. The average temperatures of the module are calculated from all cell temperatures for each U_{mod} and are given in Table 1. The temperature increased significantly from $U_{\text{mod}}=33.85$ V to 38.47 V by almost 10 K for the EL measurements. Following the approach

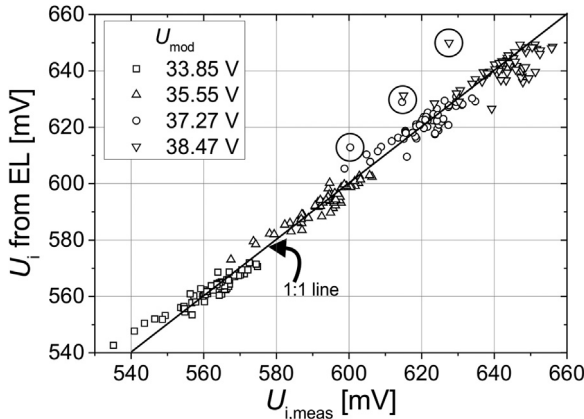


Fig. 2. Plot of measured cell voltages $U_{i,\text{meas}}$ versus cell voltages U_i . The 1:1 line is a guide for the eye and marks the curve if $U_{i,\text{meas}}$ and U_i would be equal.

of Köntges and Potthoff [23,24] the calibration constant C and the recombination coefficient B have been calculated from the measurement at 33.85 V and 0.627 A, which is well below $0.1I_{sc}$ of the module ($I_{sc}=9.37$ A) and account to $C=3.46 \times 10^{-7}$ and $B=5.74 \times 10^{-27} \text{ cm}^6$, respectively.

The calibration constants C for the higher module voltages have been calculated using Eq. (7) and are given in Table 1. With these C values the U_i have been calculated for all cells in the module by consecutively using Eqs. (4), (5), and (6) with the individual cell temperatures T_i (see Table 1 for R_{mod}). For all module voltages all U_i are plotted in Fig. 2 versus the measured voltages $U_{i,\text{meas}}$, the 1:1 line, i.e. the line showing the case $U_i=U_{i,\text{meas}}$, is plotted as a guide for the eyes.

The relative errors of each cell voltage in mV evaluated from the EL image in comparison to the respective corresponding measured voltages are shown in Fig. 3 for all module voltages. Negative relative errors means that the voltage evaluated by EL is smaller than the measured voltage (positive errors vice versa). The gray-scaled pattern in Fig. 3 illustrate the measured voltage for each cell and is scaled according to the gray scale at the top of each picture in Fig. 3. The maximum relative error is about $\pm 2\%$. However, for most of the cells the error is well below $\pm 1\%$. The voltages evaluated by EL of cells having the lowest voltages are slightly overestimated, see for instance cell No. 26, 29, and 57. The voltages of the best cells, i.e. cells with the highest voltages in the module, are slightly underestimated, see e.g. cell No. 6, 50, and 60. This holds for all module voltages. For cells No. 11 and 30, which are marked in Figs. 2 and 3 by circles, an increasing error with increasing voltage is observed, which is against the trend of all other cells. These outliers come from an increased series resistance due to the opening of the back sheet of the module. During the opening process the middle busbar was damaged or even disconnected, therefore the cell was connected to the string by only two busbars. In Fig. 1 it is observed that the EL signal at cell No. 11 at the middle busbar is clearly reduced, which is a pure series resistance effect due to the bad connection of the middle busbar to the string. Here the measured voltage is too low, since the measurement was done at the middle busbar, hence outliers emerge. The effect is not seen at the low module voltages, but is even stronger at the highest voltage, since here the high current leads to strong series resistance effects. The errors of the leftmost cells of the module are always negative (voltage from EL is determined too low) and are relatively large for the high voltage measurement. We could not figure out the reason of this effect.

3.2. Local I-V results on single cells in the module

In Fig. 4(a) a dark lock-in thermography image of the module taken at 3.8 A (37.44 V, according to the EL image in Fig. 1a) is displayed for illustration. This image is the -90° DLIT image, which is proportional to the power density dissipated in the cell [3]. The image was taken from the backside of the module, hence the junction box covers the two cells in the upper middle section of the module partly. Also the frame of the module covers some area of the edge cells, so unfortunately not all cell edges can be investigated completely, which is, however, no obstacle for the local analysis in principle. Please remember that the module was degraded. The most degraded cell in terms of the EL signal (cell No. 57) and the cell with the weakest (or almost no) degradation in terms of the EL signal (cell No. 50) are marked in Fig. 4(a) by circles. The first interesting finding is that the DLIT images of these two cells do not show distinct differences of the DLIT signal compared to the EL image in Fig. 1(a), where a clear difference between these two cells can be seen. What can be said is that the strongly degraded cell No. 57 exhibits a more homogeneous DLIT signal compared to the other cells, however the DLIT signal is almost equally strong. The reason for this unexpected behavior is that the cells are operated here in constant current mode. Hence, the poor cell No. 57 shows a higher J_{01} and thus an only slightly lower cell voltage at the same cell current, leading to nearly the same average DLIT signal. Note that the local cell voltage influences the EL signal exponentially but the DLIT signal only linearly. Therefore only for EL the individual cell temperature (i.e. averaged over the cell area) have to be regarded.

To evaluate single cells the DLIT images of the cells have been cropped accordingly to separate the DLIT images of the desired cell for each voltage. This is exemplarily shown in Fig. 4(b) for the best cell No. 50 for the three highest module voltages (cell currents, respectively). The pixel resolution of these images is about 60×60 pixels. Even though the lateral resolution is limited, still details like the pattern of the rear contact pads, which shows slightly higher DLIT signal (shown by arrows in Fig. 4(b)), can be imaged.

Normally for the Local I-V procedure DLIT images at different voltages are used, which have to be measured at one and the same temperature, usually at 25°C (298 K), to calculate reliable data. However, during the DLIT measurements of the module the cell temperatures have increased and are slightly different for each measurement (see Table 2). Nevertheless, we have applied the Local I-V analysis formally at 25°C , hence we have to correct the voltages determined from the EL images to 25°C . This approximation can be done due to the low dependence of the DLIT evaluation procedure on the actual cell temperature. Note that the DLIT-measured current densities are always scaled by the flowing current, which is well-known here. The DLIT measurement only gives information on the inhomogeneity of the current flow, which depends only weakly on temperature.

The correction of the EL evaluated and the directly measured voltages is done as follows. The cell voltages have been evaluated as described in section 4.1 from the EL images. These voltages have been determined regarding the temperature of each cell by taking a steady-state thermogram of the module during the EL measurement (see Fig. 1(d)). For the Local I-V analysis these voltages must be corrected to the values, which would be measured at e.g. 25°C (298 K). Since the EL measurements have been done at well defined constant currents, respectively (see Table 1), it is possible to correct the voltages by taking the temperature coefficient of the voltage for a given current into account. This temperature coefficient is well known and is $TC_V=-2.2 \text{ mV/K}$ for Si solar cells and it is constant in the temperature range apparent in our experiments [33]. All cell voltages measured, i.e. $U_{i,\text{meas}}$, and all from EL determined voltages U_i , have been corrected to 25°C , since this is the

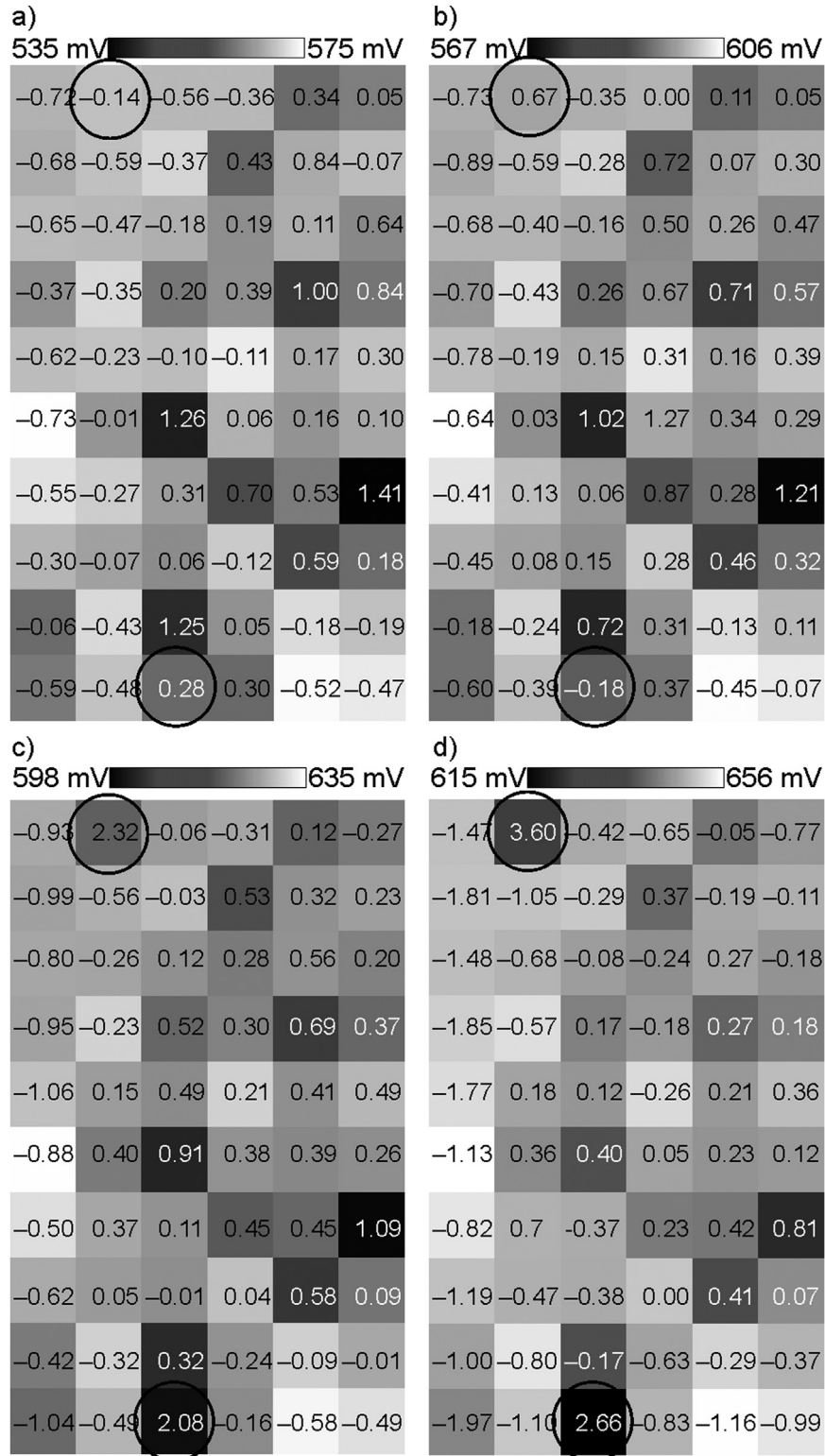


Fig. 3. Maps of the measured voltages displayed as a gray-scaled pattern of the 60 cells for the four U_{mod} : a) 33.85, b) 35.55, c) 37.27, d) 38.47. The numbers denote the relative error in % of the cell voltages determined from EL to the measured cell voltages, respectively.

temperature, which we use for the Local I-V analysis in our case. The voltages have been corrected to 298 K (25 °C) by regarding the temperature difference between 298 K and the EL temperature $T_{i,\text{EL}}$ (average over the cell area) for each cell multiplied with TC_V . This procedure is absolutely necessary to get reliable Local I-V data:

$$U_{i,\text{corr}} = U_i + (298K - T_{i,\text{EL}}[K])(TC_V). \quad (9)$$

Here $U_{i,\text{corr}}$ is the temperature-corrected voltage. Eq. (9) also holds for the Local I-V analysis using the measured voltages $U_{i,\text{meas}}$ and must be done for all cells for each measurement.

In Table 2 the measurement data of the module for the DLIT measurements are given. To illustrate the temperature differences

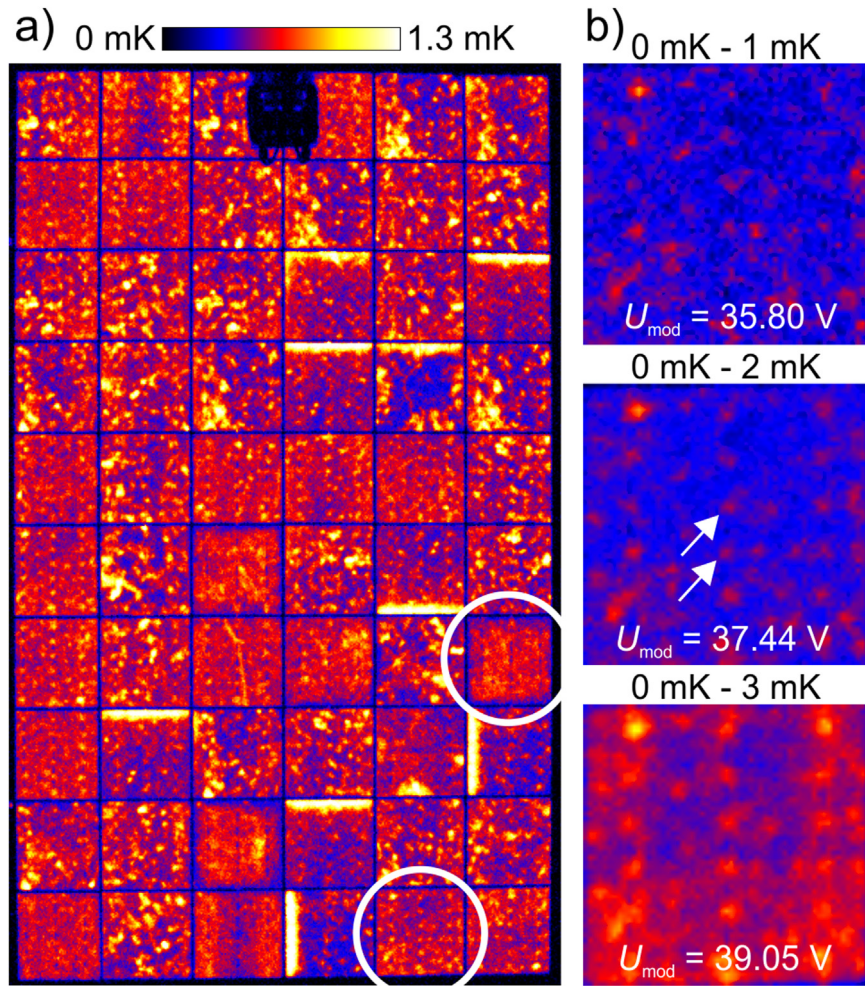


Fig. 4. a) DLIT image of the module at 37.44 V (3.8 A). b) DLIT images from cell No. 50 (the cell with the highest voltage) selected from the module DLIT images for three different module voltages. Please note the different scales in a) and b).

between the EL images and the DLIT measurement in spite of the same current, the average module temperatures are given as well as the difference between the temperatures of the EL and DLIT images. There is already a small temperature effect on the module voltages of the DLIT images: the U_{mod} during DLIT measurements are a bit higher than the module voltages of the EL measurements, at least at higher currents, caused by the slightly lower temperatures during the DLIT measurements. Please note that the module temperatures in Table 2 are average temperatures calculated from the cell temperatures derived from the thermography images taken during the measurements. Fig. 1d) shows clearly that the temperatures of the cells are different leading to slightly different temperature corrections from the EL images to 298 K, which has been taken into account for the single cell analysis as described above.

3.3. Comparison of the Local I-V analysis with $U_{i,\text{meas}}$ to the Local-IV analysis with U_i

Since we know the temperature-corrected directly measured voltages of each cell $U_{i,\text{corr, meas}}$, we can check the quality of the Local I-V evaluation with the temperature-corrected voltages $U_{i,\text{corr}}$ determined by EL by comparing them to results of the Local I-V data calculated with $U_{i,\text{corr, meas}}$. This is exemplarily shown for cell No. 24 in Fig. 5. In Fig. 5(a) from top to bottom the images of J_{01} , the U_{oc} potential, and efficiency (at U_{mpp} of the cell) calculated from the temp.-corrected measured voltages are shown, in b) the

corresponding images calculated from the temp.-corrected voltages determined by EL are displayed. U_{oc} potential means that each pixel is considered as being a homogeneous single solar cell with distinct electronic properties of this position [26]. All calculations have been done assuming 1 sun illumination ($J_{\text{sc}}=38.5 \text{ mA/cm}^2$ for our module). Please remember that these maps have been calculated with certain assumptions of the series resistance and the short circuit current and may be not the “true” maps of the respective cell parameter. However, at least we know the exact voltages from the measurement, hence we can use the maps calculated from $U_{i,\text{corr, meas}}$ as a standard for comparison to the maps calculated from $U_{i,\text{corr}}$.

The spatial resolution of the images of the cells is sufficient to distinguish structures in the cell and their characteristic behavior. In Fig. 5(c) the EL image of cell No. 24 is shown. This EL image was taken at $I_{\text{mod}}=6.705 \text{ A}$ and was cut out from the module image. In the lower left edge of cell No. 24 a cluster of recombination active defects is observed, which shows a significantly increased dark current J_{01} leading to a decreased U_{oc} and hence diminishing the efficiency, see Fig. 5(a) and (b). The resolution of our measurements is even sufficient to see the effect of the contact pads on the backside of the cell where also a decrease of U_{oc} is observable (see circles in Fig. 5(a) and (c)). The difference between the images in Fig. 5(a) and (b) is very faint and leads us to the conclusion that the Local I-V analysis using $U_{i,\text{corr}}$ is reliable. Hence, we applied the procedure to all cells in the module and checked the deviation between the calculation with $U_{i,\text{corr}}$ and the calculation with $U_{i,\text{corr}}$,

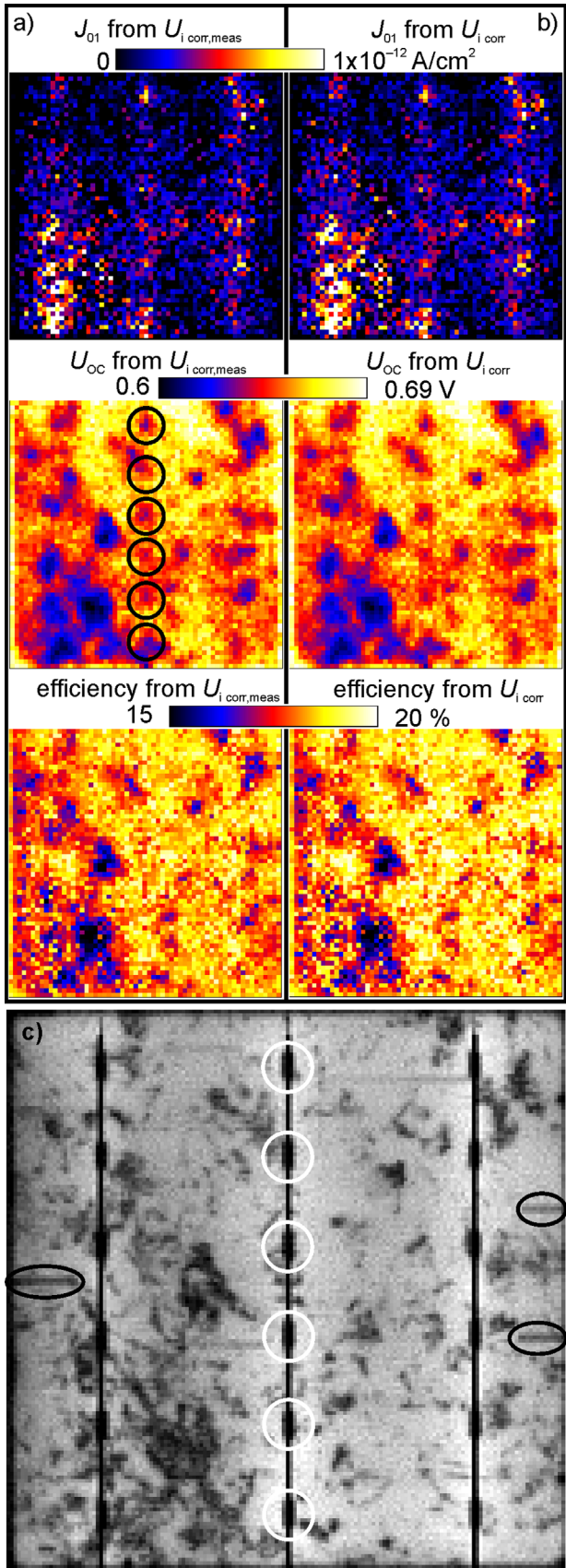


Fig. 5. a) from top to bottom: J_{01} , U_{oc} , and efficiency maps of cell No. 24 calculated with Local I-V using the temperature-corrected measured cell voltages. b) the corresponding images calculated using the temperature-corrected cell voltages determined by EL. c) EL image of cell No. 24 showing recombination active defects (dark), some grid interruptions (marked by ellipses), and the rear contact pads (marked by circles, see a).

meas.

In Fig. 6(a) the U_{oc} map of the whole module compiled from the maps calculated with $U_{i\ corr,\ meas}$ of the single cells is shown. In Fig. 6(b) the corresponding map calculated with the voltages $U_{i\ corr}$ are given. Both images are scaled to the same limits. To calculate the deviation between both images we calculated the ratio $U_{oc,i\ corr,meas}/U_{oc,i\ corr}$ and plotted it in Fig. 6(c). Absolute deviations are given in Fig. 6(d) by calculating $U_{oc,i\ corr,meas} - U_{oc,i\ corr}$. In Fig. 6(e)–(h) the same is shown for the efficiency maps. The ratios in Fig. 6(c) and (g) are scaled equally revealing that almost all cells show a deviation smaller than $\pm 2\%$ between the evaluation with $U_{i\ corr,\ meas}$ and the evaluation with $U_{i\ corr}$, which for U_{oc} leads to absolute deviations of about ± 3 to ± 5 mV and in the case of the efficiency to $\pm 0.2\%$ (abs.). At cells, which show a lower voltage than average (e.g. cell No. 57), U_{oc} and efficiency are underestimated by using $U_{i\ corr}$, at cells with voltages above the average (e.g. cell No. 50) U_{oc} and efficiency are overestimated (both cells are marked in Fig. 6 by circles). Only the results of the cells on the left edge of the module show systematically higher errors and of course cell No. 11 and 30, which was explained already above. Assuming that the Local I-V evaluation using $U_{i\ corr,\ meas}$ gives the correct cell parameters in the limits of the method (please refer [25,26]), the deviations of the results using $U_{i\ corr}$ are small and still allow quantitative analyses of single cells in modules with the combination of the voltage determination by Köntges et al. [23,24] and the Local I-V analysis [25,26].

In Fig. 6 the cells with the highest respective lowest voltages are marked by circles (cell No. 50 and 57). One can clearly see that the worst cell No. 57 has a lower U_{oc} , and a lower efficiency than all other cells. The losses are not homogeneously distributed over the cell area, the left side of the cells shows larger losses in U_{oc} for instance. Furthermore all cells showing a significant degradation effect are clearly visible in the efficiency image: cells No. 26, 29, 37, 48, and 57. Using the Local I-V analysis the losses and differences can also be quantified on cell level by regarding the global cell data from the dark and illuminated I-V curves, respectively. From the global I-V curves simulated by the Local I-V procedure all important cell parameters can be extracted for each cell. By plotting these parameters in the pattern of the cells in the module like in Fig. 3 a quick quantitative overview of the performance of single cells is possible. In Fig. 7(a)–(c) this is shown for the efficiency, the fill factor, and the cell's power (i.e. $U_{mpp} \times I_{mpp}$). Please note that these data are calculated from the EL measured $U_{i\ corr}$.

From the overview maps in Fig. 7 it is found that the span of the efficiencies of the cells is from 17.7% of the worst cell up to 19.1% of the best cell, see Fig. 7(a). The power at the maximum power point (mpp) of the cells ranges from 4.3 W to 4.6 W, please see Fig. 7(c). Accordingly the fill factors are in a typical range of 71–76%. However, please note that the fill factors are calculated with a constant and homogeneous series resistance and that ohmic shunts are not considered in our analysis, hence inhomogeneous series resistances and ohmic shunts are not reflected in the fill factor. Furthermore, the global I-V curves can be extracted from the calculated data. In Fig. 7(d) the I-V curves under illumination assuming a homogeneous $J_{sc}=38.5$ mA/cm² of cell No. 24, 50, and 57 are shown. By summing up the powers of the cells from Fig. 7(c) an estimation of the module power can be made. In the calculation each cell is set to its optimal U_{mpp} and series resistance effects due to cell interconnectors are missing, hence a slightly higher module power is expected to be calculated from the single cell powers. Thus, the calculated module power is a kind of power potential of the module, or in other words, it gives the power of the module (sum of cell powers) if there were no losses due to encapsulation, cell interconnectors in the module, and I-V curve mismatches. In our example the measured module power at mpp

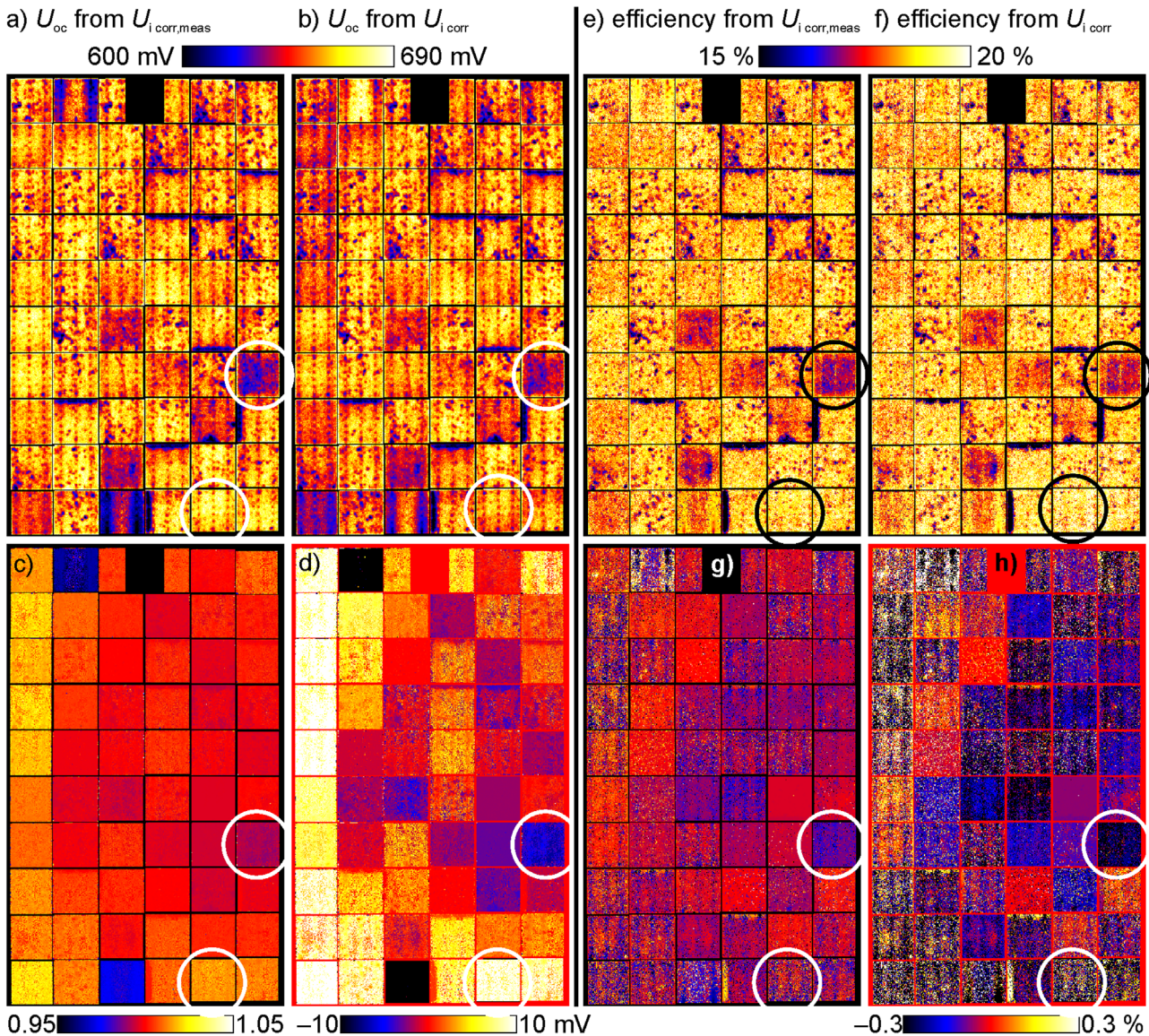


Fig. 6. U_{oc} and efficiency calculated from temperature-corrected measured voltages in a) and e), U_{oc} and efficiency calculated from temperature-corrected voltages determined with EL in b) and f), c), d) relative and absolute deviation of U_{oc} calculated from $U_{i\ corr}$, g), h) relative and absolute deviation of the efficiency calculated from $U_{i\ corr}$.

is 259.7 W, the calculated power from the Local I-V analyses by summing up the power at mpp of all cells calculated from $U_{i\ corr}$ is 269.7 W. The cell to module loss (CTM) calculates to [34]

$$CTM = \frac{\sum_{i=1}^N P_i - P_{module,meas}}{\sum_{i=1}^N P_i} * 100\% = 3.7\%, \quad (9)$$

with P_i being the single cell powers at mpp calculated from the Local I-V analysis (with temp.-corrected voltages determined from EL) and $P_{module, meas}$ is the module power from the flasher measurement. CTM calculated with the power from the Local I-V analyses done with the temp.-corrected measured voltages accounts to 2.9%, with $\sum_{i=1}^{60} P_i = 267.5$ W. Regarding the assumptions made in our analysis (constant J_{sc} and homogeneous series resistance) and keeping in mind the deviations of $U_{i\ corr}$ to $U_{i\ corr,meas}$ the value of 3.7% calculated using $U_{i\ corr,meas}$ is a good approximation. Both CTM values of our experiment are in good agreement with findings in literature, where CTM is given in a range between 1.5% and 3.3% [34,35].

3.4. Automation of the analysis

The above described method to analyze PV modules manually is somewhat lengthy and a lot of operating errors can be made during the process. Therefore we decided to automate the analyses, which makes the complete procedure much faster and very reliable for avoiding simple operation errors. The computer program solves the following tasks: i) finding the positions of the cells in the images of the module by pattern recognition, ii) determining the maximum EL signal in each cell considering outliers, iii) calculating the cell voltages and correcting them to 25 °C, iv) applying the Local I-V analysis to each cell, and finally v) calculating the I-V curves for each cell. The output is the same as described in Sections 3.2 and 3.3 and comprises all results which can be calculated with the Local I-V analysis [26]. Given that all measurement data are present, the manual evaluation took at least one to two working days (for a trained person), the automatic evaluation for a full analysis (including the calculation of all I-V curves) takes less than 5 min. The computer program named Single Cell Analysis in Modules (SCAM) will be made available from the authors soon. We have tested the program with data presented in this

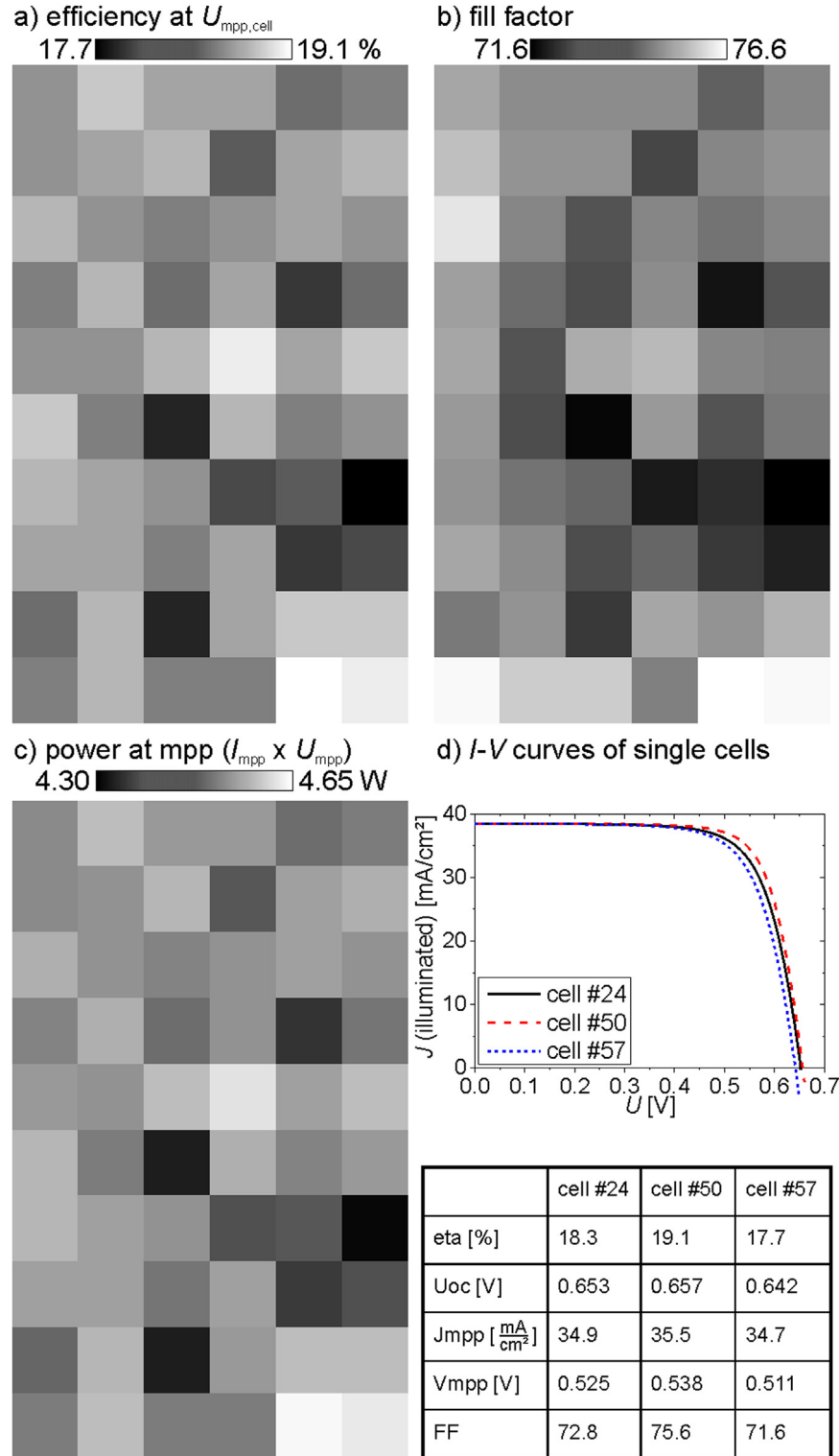


Fig. 7. Maps of solar cell performance parameter: a) cell efficiency calculated at the cell's U_{mpp} , b) the fill factor, and c) the maximum cell power. In d) the calculated illuminated I-V curves and global solar cell parameters of three cells with very different performance are shown (simulation done with homogeneous series resistance of $0.7 \Omega \text{ cm}^2$ and homogeneous short circuit current of $38.5 \text{ mA}/\text{cm}^2$).

contribution. As a rule, the deviations to the manually obtained results are much less than $\pm 1\%$. Hence there is no practical difference between the automatic and the manual analysis if one considers that also the manual analysis is somehow prone to errors as described above and will be discussed below.

4. Discussion

In the course of our experiments, it turned out that the measurement of the temperatures of the cells, respective module, is very important to get reliable results for the voltages from the EL measurements. Since the voltages are an important input for the Local I-V analysis, care was taken to reduce the influence of

temperature deviations in our experiments. Normally it is required to perform all measurements at the same temperature to get reliable data, especially if quantitative results are desired. However, experimentally it is very elaborate or even impossible to hold the whole module under a constant temperature during all measurements. This is aggravated by the fact that the DLIT measurements are done under different power consumptions compared to the EL measurements due to the pulsed voltage supply during DLIT. Hence each measurement was done at a different temperature, which must be corrected accordingly to the purposes of the analyses. In our experiments it turned out that a correction of the voltages from the EL measurement to a constant temperature which we use (typically 25 °C) for the Local I-V evaluation is necessary to get reliable results. Of course each correction procedure produces some error and may be detrimental to the results. To check the reliability of our approach we compared the evaluation of the voltages determined by EL and the results from the Local I-V analyses with the measured voltages and the corresponding Local I-V results. It turned out that deviations of about $\pm 1\%$ of the voltages (about ± 5 to ± 7 mV), leads still to reliable Local I-V results with deviations of about $\pm 2\%$ (i.e. for example ± 5 mV for U_{oc}), compared to the analyses done with measured voltages (see Fig. 6). As already found by Köntges et al. and Potthoff et al. [23,24] the voltages of cells with low performance are systematically overestimated, and cells with high performance are systematically underestimated. We believe that this is a result of the assumption of the Köntges/Potthoff method [23,24] that each cell shows at least one good region. This is probably not correct for the "LeTID" degraded cells [13] of our module, since this degradation mode is known to appear homogeneously. However, we found that even these deviations do not prevent a meaningful Local I-V analysis of single cells. It must be considered that approximations of the series resistance R_s and the short circuit current J_{sc} for all cells have to be made to perform a Local I-V analysis. These are the only parameters which have to be estimated. For both parameters the same constant and homogeneous values for all cells have been taken, respectively. At first for the efficiency parameter estimation one has to assume a constant J_{sc} , which is not realistic, but this value can be taken from the flasher measurement of the module and represents only a small error. This J_{sc} is kind of a mean J_{sc} of the module. In principle it is possible to calculate J_{sc} maps from the DLIT data for each cell based on the J_{01} data [36]. However, for this procedure the global J_{sc} of each cell is necessary to know, which is not possible so far for cells embedded in modules. Hence the method of using individual J_{sc} maps for Local I-V is not applicable to single cells in modules at the present stage of this study. Furthermore, a typical constant and homogeneous series resistance of the cells have to be assumed, which is definitively a stronger error. Hence, also grid interruptions such as those marked in the EL image in Fig. 5(c) can not be analyzed. However, so far it is not possible to get series resistances of single cells out of the measurements done, without destroying the module (e.g. open the backside to contact the solar cells).

The Local I-V results of most of the cells are reliable, but there are some outliers. First of all the outliers at cell No. 11 and 30 are purely due to experimental handling. Here the middle busbar has been damaged so strongly during the contacting that reliable data is not achievable from this cells. However, normally the method presented here does not require an opening of the rear side, hence such errors are not to be expected in a module analysis following our approach. Some cells in the module showed larger deviations compared to the rest. These cells are the cells on the left edge of the module, see Figs. 3 and 6. In Fig. 3 it becomes obvious that the voltages are systematically underestimated in comparison to the other cells. This leads to a higher deviation in the Local I-V analyses of about +3% to +4%. Especially the U_{oc} determination was

erroneous due to the too low voltages, see Figs. 3 and 6. Other cell parameters deviate not that strong from the analyses with measured voltages, so we still use them for the analysis of the module, e.g. for the power evaluation. Unfortunately until now we could not figure out where this systematical error comes from. It might be suspected that the temperature measurement at this edge of the module was not as correct as desired, maybe due to thermal reflections of the surrounding or the room ventilation occasionally cooling this side of the module gently (see Fig. 1(d) where the module's left side is slightly cooler than the rest of the module).

5. Conclusion

With a combination of the voltage determination of single cells in PV modules by electroluminescence imaging [23,24] and the Local I-V evaluation with dark lock-in thermography of single cells [25,26] we were able to characterize all cells of a 60 cell module quantitatively. We measure the terminal voltages of all cells at the middle busbar by opening the back sheet of the module locally, ensuring the integrity of the module, hence we assume to perform a quasi non-destructive direct voltage measurement. The measured cell voltages give us the possibility to check the quality of the approach of voltage determination by EL images and subsequent Local I-V analysis using DLIT images. The deviation between measured voltages and voltages calculated from the EL images was about $\pm 1\%$, i.e. about ± 5 to ± 7 mV, leading to a deviation of the Local I-V results of about $\pm 2\%$. Hence, with our approach it is possible to calculate single I-V curves of solar cells in modules and to calculate the performance of single cells quantitatively. The Local I-V evaluation allows us to map the cell parameters such as J_{01} , U_{oc} , P_{mpp} , efficiency, FF, and so forth of each cell. It is possible to determine the efficiency of cells with an accuracy of less than $\pm 0.2\%$ (abs.) and U_{oc} with an accuracy of about ± 3 mV compared to the evaluation with measured voltages. Hence with our method the power and the performance degradation of single cells in modules can be determined reliably with a good spatial resolution, which was 2.6 mm per pixel in our case with a 640×512 pixels DLIT camera imaging the whole module. The spatial resolution can be improved by taking pictures of only a part of the module.

Funding

This work was supported by the German Federal Ministry for Economic Affairs and Energy and by the industry partners within the Research Cluster Solar LIFE under Contract no. 0325763D. The authors are responsible for the content.

Acknowledgment

F. Kersten and K. Petter from Hanwha Q Cells are acknowledged for providing the special prepared module and module data. We thank InfraTec GmbH for providing and further developing the PV-LIT system used for the DLIT investigations.

References

- [1] T. Trupke, J.W. Weber, Luminescence imaging: a powerful characterization tool for photovoltaic applications, in: Proceedings of the SPIE 7772, 2010, 777202.
- [2] T. Fuyuki, H. Kondo, T. Yamazaki, Y. Takahashi, Y. Uraoka, Photographic surveying of minority carrier diffusion length in polycrystalline silicon solar cells by electroluminescence, *Appl. Phys. Lett.* 86 (2005) 262108.
- [3] O. Breitenstein, M. Langenkamp, W. Warta, Lock-in Thermography - Basics and

- Use for Evaluating Electronic Devices and Materials, second ed., Springer, Berlin Heidelberg, 2010.
- [4] B.L. Sopori, A. Baghdadi, Some investigations on the influence of defects/grain boundaries on photovoltaic mechanisms in polycrystalline silicon films, *Sol. Cells* 1 (1979/1980) 237–250.
- [5] B. Moralejo, M.A. González, J. Jiménez, V. Parra, O. Martínez, J. Gutiérrez, O. Charro, LBIC and reflectance mapping of multicrystalline Si solar cells, *J. Electron. Mat.* 39 (2010) 663–670.
- [6] J. Carstensen, G. Popkirov, J. Bahr, H. Föll, CELLO: an advanced LBIC measurement technique for solar cell local characterization, *Sol. Energy Mater. Sol. Cells* 76 (2003) 599–611.
- [7] S. Kajari-Schröder, I. Kunze, U. Eitner, M. Köntges, Spatial and orientational distribution of cracks in crystalline photovoltaic modules generated by mechanical load tests, *Sol. Energy Mater. Sol. Cells* 95 (2011) 3054–3059.
- [8] P. Chaturvedi, B. Hoex, T.M. Walsh, Broken metal fingers in silicon wafer solar cells and PV modules, *Sol. Energy Mater. Sol. Cells* 108 (2013) 78–81.
- [9] S.V. Spataru, D. Sera, P. Hacke, T. Kerekes, R. Teodorescu, Fault identification in crystalline silicon PV modules by complementary analysis of the light and dark current–voltage characteristics, *Prog. Photovolt.: Res. Appl.* (2015), <http://dx.doi.org/10.1002/pip.2571>.
- [10] S. Pingel, O. Frank, M. Winkler, S. Oaryan, T. Geipel, H. Hoehne, J. Berghold, Potential induced degradation of solar cells and panels, in: Proceedings of the 35th IEEE Photovolt. Specialists Conf. (PVSC), Honolulu, HI, USA, 2010, pp. 002817–002822, <http://dx.doi.org/%2010.1109/PVSC.2010.5616823>.
- [11] M. Schütze, M. Junghänel, M.B. Koentopp, S. Cwikla, S. Friedrich, J.W. Müller, P. Wawer, Laboratory study of potential induced degradation of silicon photovoltaic modules, in: Proceedings of the 37th IEEE Photovolt. Specialists Conference (PVSC), Seattle, WA, USA, 2011, pp. 000821–000826, <http://dx.doi.org/%2010.1109/PVSC.2011.6186080>.
- [12] M.B. Koentopp, M. Krober, C. Taubitz, Toward a PID test standard: understanding and modeling of laboratory tests and field progression, *IEEE J. Photo.* 6 (2016) 252–257, 2016.
- [13] F. Kersten, P. Engelhart, H.-C. Ploigt, A. Stekolnikov, T. Lindner, F. Stenzel, M. Bartczsch, A. Szpetz, K. Petter, J. Heitmann, J.W. Müller, A New mc-Si Degradation Effect called LeTID, in: Proceedings of the 42nd IEEE Photovolt. Specialists Conf. (PVSC), New Orleans, LA, USA, 2015, pp. 1–5, <http://dx.doi.org/%2010.1109/PVSC.2015.7355684>.
- [14] J. Berghold, M. Roericht, A. Böttcher, S. Wendlandt, M. Hanusch, S. Koch, P. Grunow, B. Stegemann, Electrochemical corrosion within solar panels, in: Proceedings of the 27th European Photovoltaic Solar Energy Conference and Exhibition (EUPVSEC), Frankfurt, Germany, 2012, pp. 3511–3517, <http://dx.doi.org/%2010.4229/27thEUPVSEC2012-4BV.3.37>.
- [15] R. Khatri, S. Agarwal, I. Saha, S. Kumar Singh, B. Kumar, Study on long term reliability of photovoltaic modules and analysis of power degradation using accelerated aging tests and electroluminescence technique, *Energy Procedia* 8 (2011) 396–401.
- [16] M. García, L. Marroyo, E. Lorenzo, J. Marcos, M. Pérez, Observed degradation in photovoltaic plants affected by hot-spots, *Prog. Photovolt.: Res. Appl.* 22 (2014) 1292–1301.
- [17] S. Wendlandt, A. Giese, A. Drobisch, D. Tornow, M. Hanusch, J. Berghold, S. Krauter, P. Grunow, The temperature as the real hot spot risk factor at PV-modules, in: Proceedings of the 27th European Photovoltaic Solar Energy Conference and Exhibition (EUPVSEC), Frankfurt, Germany, 2012, pp. 3553–3557, <http://dx.doi.org/%2010.4229/27thEUPVSEC2012-4BV.3.52>.
- [18] T. Kaden, K. Lammers, H.J. Möller, Power loss prognosis from thermographic images of PID affected silicon solar modules, *Sol. Energy Mater. Sol. Cells* 142 (2015) 24–28, 2015.
- [19] C. Buerhop, R. Auer, C. Brabec, Characterizing PV-modules with a new IR-EL-camera, in: Proceedings of the 28th European Photovoltaic Solar Energy Conference and Exhibition (EUPVSEC), Paris, France, 2013, pp. 3243–3245, <http://dx.doi.org/%2010.4229/28thEUPVSEC2013-4AV.5.24>.
- [20] U. Hoyer, C. Buerhop, Electroluminescence and infrared imaging for quality improvements of PV modules, in: Proceedings of the 23th European Photovoltaic Solar Energy Conference and Exhibition (EUPVSEC), Valencia, Spain, 2008, pp. 2913–2916.
- [21] R. Ebner, S. Zamini, G. Újvári, Defect analysis in different photovoltaic modules using electroluminescence (EL) and infrared (IR)-Thermography, in: Proceedings of the 25th European Photovoltaic Solar Energy Conference and Exhibition (EUPVSEC)/5th World Conference on Photovoltaic Energy Conversion, Valencia, Spain, 2010, pp. 333–336.
- [22] F. Fröhlauf, M. Turek, Quantification of electroluminescence measurements on modules, *Energy Procedia* 77 (2015) 63–68.
- [23] M. Köntges, M. Siebert, D. Hinken, U. Eitner, K. Bothe, T. Potthoff, Quantitative analysis of PV-modules by electroluminescence images for quality control, in: Proceedings of the 24th European Photovoltaic Solar Energy Conference and Exhibition (EUPVSEC), Hamburg, Germany, 2009, pp. 3226–3231, <http://dx.doi.org/%2010.4229/24thEUPVSEC2009-4CO.2.3>.
- [24] T. Potthoff, K. Bothe, U. Eitner, D. Hinken, M. Köntges, Detection of the voltage distribution in photovoltaic modules by electroluminescence imaging, *Prog. Photovolt.: Res. Appl.* 18 (2010) 100–106.
- [25] O. Breitenstein, Nondestructive local analysis of current–voltage characteristics of solar cells by lock-in thermography, *Sol. Energy Mater. Sol. Cells* 95 (2011) 2933–2936.
- [26] O. Breitenstein, Local efficiency analysis of solar cells based on lock-in thermography, *Sol. Energy Mater. Sol. Cells* 107 (2012) 381–389.
- [27] Search for Local I–V, <http://www.max-planck-innovation.de>, 2016 (accessed).
- [28] A.W. Blakers, A. Wang, A.M. Milne, J. Zhao, M.A. Green, 22.8% efficient silicon solar cell, *Appl. Phys. Lett.* 55 (1989) 1363–1365.
- [29] P. Würfel, T. Trupke, T. Puzzer, E. Schäffer, W. Warta, S.W. Glunz, Diffusion lengths of silicon solar cells from luminescence images, *J. Appl. Phys.* 101 (2007) 123110.
- [30] K. Bothe, D. Hinken, Quantitative luminescence characterization of crystalline silicon solar cells, *Semicond. Semimet.* 89 (2013) 259–339.
- [31] A.B. Sproul, M.A. Green, Improved value for the silicon intrinsic carrier concentration from 275 to 375 K, *J. Appl. Phys.* 70 (1991) 846.
- [32] K. Misiakos, D. Tsamakis, Accurate measurements of the silicon intrinsic carrier density from 78 to 340 K, *J. Appl. Phys.* 74 (1993) 3293.
- [33] O. Dupré, R. Vaillon, M.A. Green, Physics of the temperature coefficients of solar cells, *Sol. Energy Mater. Sol. Cells* 140 (2015) 92–100.
- [34] H. Yang, H. Wang, D. Cao, D. Sun, X. Ju, Analysis of power loss for crystalline silicon solar module during the course of encapsulation, *Int. J. Photo.* (2015) 1–5.
- [35] M.B. Koentopp, M. Schütze, D. Buß, R. Seguin, Optimized module design: a study of encapsulation losses and the influence of design parameters on module performance, *IEEE J. Photovolt.* 3 (2013) 138–142.
- [36] O. Breitenstein, F. Fertig, J. Bauer, An empirical method for imaging the short circuit current density in silicon solar cells based on dark lock-in thermography, *Sol. Energy Mater. Sol. Cells* 143 (2015) 406–410.